Journal of Computational Physics: X 17 (2023) 100128

Contents lists available at ScienceDirect

Journal of Computational Physics: X

journal homepage: www.elsevier.com/locate/jcpx

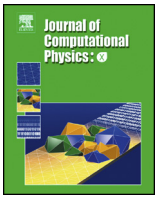

Natural grid stretching for DNS of compressible wall-bounded flows

Alessandro Ceci *, Sergio Pirozzoli

Dipartimento di Ingegneria Meccanica e Aerospaziale, Sapienza Università di Roma, Via Eudossiana 18, Roma 00184, Italy

ARTICLE INFO

Article history:
Received 23 November 2022
Received in revised form 28 April 2023
Accepted 24 May 2023
Available online 30 May 2023

Keywords:
Direct numerical simulation
Wall turbulence
Compressible flows

ABSTRACT

We propose a physics-driven stretching function for direct numerical simulation (DNS) of compressible turbulent wall-bounded flows, which blends uniform near-wall spacing with uniform resolution in terms of semi-local Kolmogorov units in the outer wall layer. Given target Mach number, Reynolds number and wall temperature, our procedure yields a well-defined prescription for the number of grid points and their distribution which guarantee at the same time numerical accuracy and judicious exploitation of computational resources. DNS of high-speed turbulent boundary layers are used to evaluate the quality of the proposed stretching function, which show that one can achieve identical results as with general-purpose stretching functions, however with substantially higher efficiency. A Python script is provided to facilitate implementation of the proposed grid stretching.

1. Introduction

Direct numerical simulation (DNS) of wall-bounded flows is by now an established practice, started from the pioneering work of Kim et al. [1] for channel flow. Although meshing may not be challenging for the simple topology of canonical flows to which DNS is currently limited, the mesh parameters significantly affect computational accuracy and efficiency. It is generally acknowledged (e.g. Lee and Moser [2]) that mesh spacings in the order of ten wall units in the streamwise direction and five in the spanwise direction are sufficient in pseudo-spectral calculations to achieve good resolution of the buffer-layer energy-containing eddies, namely streaks and associated quasi-streamwise vortices. The buffer layer is especially important as the topology of eddies changes from sheet-like near the wall to rod-like away from it, corresponding to the inflectional point of the wall-normal velocity variance profile [3]. Finite-difference schemes require similar or slightly higher number of grid points [4], to achieve the same quality of results. More disputable is the selection of the mesh properties in the wall-normal direction, which is strongly anisotropic for the flow, and for which no rule is consolidated yet. In fact, different authors of state-of-art DNS have used vastly different mapping functions, and the selection of the total number of grid points remains a matter of personal experience and feeling. In a recent work, Pirozzoli and Orlandi [5] proposed a natural wall-normal grid mapping for incompressible flows, providing a definite prescription for the number of grid points and near-wall grid clustering needed to achieve accurate results with judicious exploitation of computational resources.

In compressible flows, for which DNS is now also well established [6–13], difficulties in proper meshing are exacerbated by the change of the mean thermodynamic and transport properties across the wall layer, which make extrapolation of tools borrowed from incompressible turbulence far from straightforward. The purpose of this paper is to derive stretching

* Corresponding author.
E-mail address: alessandro.ceci@uniroma1.it (A. Ceci).

https://doi.org/10.1016/j.jcpx.2023.100128

functions for DNS of compressible boundary layers which are targeted to an arbitrary set of Mach and Reynolds number and wall temperature. Although the forthcoming discussion is mainly focused on the case of turbulent boundary layers, other canonical cases can also be handled with no or minimum modifications, as pipe and plane channel flows.

2. Wall-normal stretching functions

Considerations about the multi-scale nature of wall-bounded turbulence lead to conclude that several constraints shall be satisfied for effective design of the wall-normal mapping function: i) the first off-wall grid node (say Δy_w^+) shall be placed close enough that the severe velocity gradients occurring in that region are resolved, which requires $\Delta y_w^+ \lesssim 1$; ii) grid points should be conveniently clustered within the buffer layer (say, $y^+ \leq 50$) which is the most anisotropic region of the flow, and in which most intense phenomena occur; iii) the spacing in the outer part of the wall layer, in which turbulence is close to isotropic, should be of the order of the local Kolmogorov length scale (η). Close to the wall $\eta^+ \approx 1.5$ [14], hence requirement i) is more restrictive than iii). In the outer region, near balance between turbulence kinetic energy production and dissipation rates is observed, hence the key requirement for DNS is resolving eddies down to the dissipative scale. We believe that, given the near universality of wall-bounded flows, a universal treatment of the stretching function is possible and appropriate. We then reason as follows. First, following Hoyas and Jiménez [15], we believe that the grid spacing in the outer layer should be selected to be proportional to the local Kolmogorov length scale, say $\eta^+ = \varepsilon^{+-1/4}$, with ε the local dissipation rate, and $+$ denoting wall units. Hence, the first requirement which we set is that the local grid spacing in the outer layer should be $\Delta y^+ = \alpha \eta^+$, with α controlling adequate resolution of the dissipative eddies. The choice $\alpha = 2.0$ yields a resolution in spectral space $k_{max}\eta \approx 1.5$ (where $k_{max} = \pi/\Delta y$ is the maximum resolved wavenumber) which, although a bit less than used in previous DNS of isotropic turbulence [16], and of channel flow [15], yields very good prediction of all key statistics, as shown below. We will also assess the influence of the parameter α, by increasing its value up to 3.25. In their study, Pirozzoli and Orlandi [5] assumed $\alpha \approx 1.25$, whereas other studies considered values in the range $\alpha \approx 1.25 - 1.5$, which is regarded to be sufficient for numerical simulations of isotropic turbulence and wall-bounded flows [16,15,1,2,17–20]. According to Pope [21], the dissipation spectrum is very small beyond $k\eta = 1.5$, hence $k_{\max}\eta \approx 1.5$ guarantees good resolution of the dissipative scales. In physical space, the resulting wall-normal spacing is $\Delta y/\eta = \pi/1.5 \approx 2.1$. The aforementioned restrictions apply identically to incompressible flow and to the solenoidal part of the velocity field in compressible flow. In the latter case dilatational structures also have dynamical relevance [22], whose resolution could be more challenging than for the solenoidal part of the flow, but this is disregarded in the present work. In incompressible flow, the equilibrium conditions in the log layer yield $\epsilon^+ \sim 1/y^+$, hence it follows [14] that

$$\eta^+ \approx c_\eta y^{+1/4}, \tag{1}$$

with $c_\eta = \kappa^{1/4} \approx 0.8$ (κ is the von Kármán constant), which is consistent with all available DNS of channel and pipe flow. Thus, let j be the wall-normal grid index (momentarily assumed to be continuous for convenience), we require that

$$\Delta y^+ = \frac{\mathrm{d}y^+}{\mathrm{d}j} = \alpha c_\eta y^{+1/4}, \tag{2}$$

which upon integration yields

$$y^+(j) = \left(\frac{3}{4}\alpha c_\eta j\right)^{4/3}, \tag{3}$$

which defines the mesh stretching in the outer wall layer. Next to the wall, in the viscous sublayer the mean velocity gradient is nearly constant up to $y^+ \approx 5$, and use of uniform spacing is appropriate, hence

$$y^+(j) = \Delta y_w^+ \cdot j. \tag{4}$$

A smooth blending between the near-wall mapping (4) and the outer-layer mapping (3) is further assumed, to yield

$$y^+(j) = \frac{1}{1+(j/j_b)^2}\left[\Delta y_w^+ j + \left(\frac{3}{4}\alpha c_\eta j\right)^{4/3}(j/j_b)^2\right], \tag{5}$$

where the parameter j_b defines the grid index at which transition between the near-wall and the outer mesh stretching occurs. The above reasoning needs to be significantly modified for adaptation to compressible flow, as we discuss below.

Direct numerical simulations of compressible flow are typically carried out with standard stretching functions, and selecting the number of grid points based on personal experience and grid-sensitivity studies. This is well reflected in Table 1, which shows available information about previous representative DNS of compressible boundary layers. As one can notice, different studies rely on different mapping functions (see Orlandi [25] for an overview of classical ones), different near-wall resolutions, and even very different total number of points for similar flow conditions. We believe that setting standard

Table 1
List of mesh parameters for reference DNS studies of compressible turbulent boundary layers. Here $Re_\tau = u_\tau \delta/\nu$ (with u_τ the friction velocity, δ the boundary layer thickness, and ν the fluid kinematic viscosity) is the friction Reynolds number, N_y is the number of collocation points in the wall-normal direction, M_0 is the free-stream Mach number, T_w/T_r is the wall to recovery temperature ratio and Δy_w is the distance of the first off-wall node. INSF refers to the natural stretching function for incompressible flow given in Eq. (5) (Pirozzoli and Orlandi [5]).

Reference	Stretching function	M_0	T_w/T_r	Re_τ	N_y	Δy_w^+
Duan et al. [6]	geometrical	5	0.18	798	110	0.33
			0.35	625		0.32
			0.53	522		0.33
			0.68	434		0.33
			adiabatic	386		0.30
Duan et al. [7]	geometrical	0.3	adiabatic	570	110	0.10
		3		487		0.30
		5		416		0.25
		7		392		0.27
		12		377	120	0.27
Lagha et al. [8]	hyperbolic	2.5	adiabatic	340	128-180	0.3
		5		300		
		7.5		310		
		10		300		
		15		302		
		20		345		
Pirozzoli and Bernardini [9] Pirozzoli and Bernardini [23]	hyperbolic	2	adiabatic	205-273	171	0.60
				448-591	221	0.70
				843-1123	331	0.70
				3413-3955	900	0.90
Wenzel et al. [10]	NA	0.3	adiabatic	237-943	240	0.66-0.81
		0.5		237-943		0.64-0.79
		0.7		233-922		0.60-0.73
		0.85		215-827		0.57-0.69
		1.5		182-620		0.41-0.50
		2		158-482		0.31-0.37
		2.5		140-369		0.23-0.27
Zhang et al. [11]	hyperbolic	2.5	adiabatic	510	400	0.6
		5.84	0.25	450	560	0.46
		5.86	0.76	453	500	0.51
		7.87	0.48	480	600	0.55
		13.64	0.18	646	540-786	0.47
Huang et al. [12]	NA	2.5	adiabatic	395-1199	680	0.51
		4.9	0.91	726-1244	550	0.53
		10.9	0.2	672–1193	500-690	0.43
Cogo et al. [13]	INSF	2	0.76	340–620	320	0.5
				1240–2300	832	0.7
		5.86		290–520	320	0.5
				1080–1953	832	0.7
Ceci et al. [24]	hyperbolic	2	adiabatic	374-473	512	0.6
				559-707		
				772-992		
	INSF	5.84	0.25	527-654	352	0.4
				687-844		
				905-1115		

guidelines for the choice of the wall-normal stretching function is appropriate, also in the interest of minimizing the computational effort.

For that purpose, the main assumption which we will exploit is universality of the distribution of η in terms of semi-local wall units [26–29], namely units based on the local friction velocity, $u_\tau^* = (\tau_w/\rho)^{1/2}$, and the local viscous length scale, $\delta_v^* = \nu/u_\tau^*$. Normalization with semi-local wall units is hereafter denoted with the asterisk symbol. The relationship with the standard wall units is as follows, $u_\tau^* = u_\tau R^{-1/2}$, $\delta_v^* = M R^{-1/2} \delta_v$, where $M = \mu/\mu_w$, $R = \rho/\rho_w$, are the local to wall viscosity and density ratios, respectively. Our ansatz then translates into

$$\eta^* = \eta^+(y^*), \tag{6}$$

where

$$y^* = y^+ R^{1/2}/M, \quad \eta^* = \eta^+ R^{1/2}/M, \tag{7}$$

Table 2
List of computational parameters for the present DNS campaign. NSF refers to the proposed natural stretching function, and HSF refers to hyperbolic sine stretching function. Here δ_0 is the inflow boundary layer thickness, L_x, L_y, L_z are the streamwise, wall-normal and spanwise extensions of the computational domain, with N_x, N_y, N_z being the respective number of collocation points. $\Delta x, \Delta z$ are the uniform streamwise and spanwise spacings, and $N_{y,\delta}$ is the number of grid points in the wall-normal direction up to the boundary layer edge.

Flow case	M_0	T_w/T_r	Re_τ	L_x/δ_0	L_y/δ_0	L_z/δ_0	Δx^+	Δy_w^+	Δz^+	$N_x \times N_y \times N_z$	$N_{y,\delta}$
M2-NSF	2.00	adiabatic	610	150	8	9	7.9	0.50	3.4	$4016 \times 272 \times 560$	178
M2-HSF	2.00	adiabatic	610	150	8	9	7.9	0.50	3.4	$4016 \times 368 \times 560$	293
M6-NSF	5.84	0.25	730	150	10	9	7.4	0.50	3.9	$5024 \times 288 \times 560$	171
M6-HSF	5.84	0.25	730	150	10	9	7.4	0.50	3.9	$5024 \times 496 \times 560$	384

which will be empirically tested based on DNS data. A solid plausibility argument for this ansatz involves analysis of the behavior in the log layer in compressible flow. Assuming balance between turbulence kinetic energy production and dissipation it is straightforward to arrive at the following prediction for the Kolmogorov length scale

$$\eta^+ = \frac{M^{3/4}}{R^{3/4}} \varepsilon^{+-1/4} = \frac{M^{3/4}}{R^{3/8}} (\kappa y^+)^{1/4}. \tag{8}$$

When cast in semi-local units, the previous expression becomes

$$\eta^* = (\kappa y^*)^{1/4}, \tag{9}$$

which is identical to the incompressible relation (1).

Hence, following up on Eq. (5), we assume the following distribution of the grid points in semi-local units,

$$y^*(j) = \frac{1}{1 + (j/j_b)^2} \left[j \, \Delta y_w^* + \left(\frac{3}{4} \alpha^* c_\eta j \right)^{4/3} (j/j_b)^2 \right], \tag{10}$$

with α^* a parameter controlling the resolution away from walls, and with associated distribution of grid spacings,

$$\Delta y^*(j) = \frac{\mathrm{d}y^*}{\mathrm{d}j} = \frac{1}{\left(1 + (j/j_b)^2\right)^2} \left[\left(1 - (j/j_b)^2\right) \Delta y_w^* + \frac{2}{3} \left(\frac{3}{4} \alpha^* c_\eta \right)^{4/3} \frac{j^{7/3}}{j_b^2} \left(5 + 2(j/j_b)^2\right) \right]. \tag{11}$$

The main difficulty with applying the above mappings is that the resolution requirement should be enforced in terms of the physical grid spacing, namely $\Delta y^+(j) \leq \alpha \eta^+$, for given constant α, for all j. Since $\Delta y^+(j) = \Delta y^*(j) \, \mathrm{d}y^+/\mathrm{d}y^*$, this implies that

$$\Delta y^*(j) \leq \alpha \eta^* \frac{M}{R^{1/2}} \frac{\mathrm{d}y^*}{\mathrm{d}y^+}, \quad \forall j, \tag{12}$$

Eq. (12) is satisfied. Once the optimal value α^*_{opt} is determined, the distribution of the grid points in Eq. (10) can be finally mapped back to physical space through Eq. (7).

Key ingredients in the previous developments are the distributions of the mean density and viscosity, as expressed by functions M and R, which in compressible flow depend on the exterior flow conditions and wall state. Although no exact solution is available, accurate estimates of the mean velocity, temperature and viscosity profiles, for given Mach and Reynolds number and wall thermal condition have been derived by Kumar and Larsson [30], based on numerical integration of the turbulent boundary layer equations with Prandtl mixing length closure [31], and use of Coles wake function [32], upon application of an inverse compressibility transformation [33], which was found to be accurate for high-speed boundary layers across a range of Mach and Reynolds numbers and wall temperatures [30]. Alternative transformations could possibly be considered for internal flows, namely channels and pipes. This will the basis for the development of our natural stretching function (NSF). The first off-wall node is specified in terms of the Δy_w^+ parameter, and the corresponding Δy_w^*, is evaluated using the near-wall derivative of R and M. In DNS of compressible boundary layers the most restrictive time step limitation is the CFL conditions for acoustic waves at the wall, which implies that one should decide Δy_w^+ by compromising between accuracy and feasibility of the simulations [34]. Values of $\Delta y_w^+ \approx 0.5$, turn out to be an effective choice according to our numerical experiments.

Regarding the selection of the grid spacing in the wall-parallel directions, in a standard structured mesh those are partitioned uniformly, with spacings selected such that restrictions based on experience with incompressible wall turbulence are satisfied, say $\Delta x^+ \approx 8$, $\Delta z^+ \approx 4$. Despite change of the mean flow properties across the boundary layer in compressible flow, we have found that this choice is still effective, hence the same resolution in wall units in the wall-parallel directions is retained for the DNS hereafter reported.

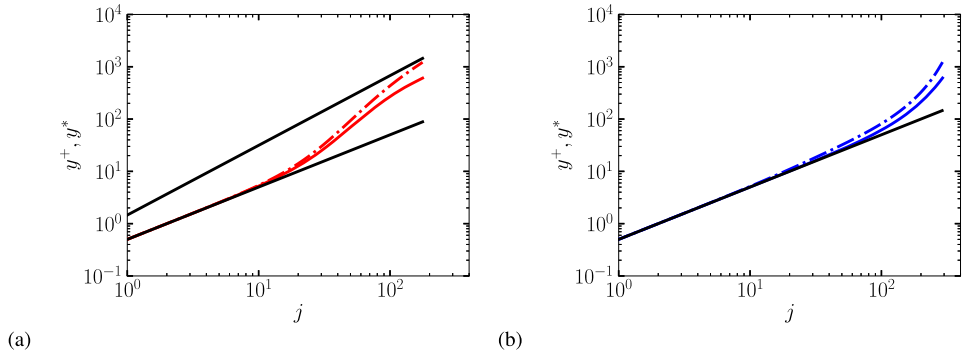

Fig. 1. Flow case M2: natural stretching function (a) and hyperbolic sine stretching function (b). The natural stretching function is designed according to Eqs. (10), (7), assuming $\Delta y_w^+ = 0.5$, $\alpha_{\rm opt}^* = 2.213$. The hyperbolic stretching is designed according to Eq. (13) with $Re_\tau = 610$ and $\beta = 3.326$. The colored solid lines refer to coordinates expressed in wall units (y^+), and the dash-dotted to coordinates expressed in semi-local units (y^*). The black lines in (a) denote the asymptotic near-wall and outer-layer stretching, and in (b) the near-wall stretching only, in wall units.

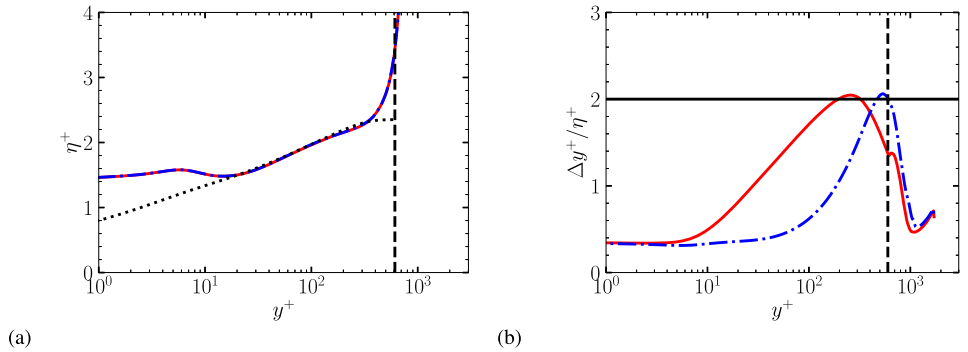

Fig. 2. Flow case M2: distribution of Kolmogorov length scale (a), and grid spacing distribution in local Kolmogorov units (b). In panel (a) the colored lines denote the distribution obtained from the DNS, and the black dotted line the prediction of Eq. (8). In both panels the red solid line indicates the NSF, the blue dash-dotted line the HSF, and the vertical dashed lines mark the boundary layer edge. In panel (b) the black horizontal line denotes the nominal resolution threshold ($\Delta y^+/\eta^+ = 2$).

3. Numerical tests

Numerical tests are here presented for two representative cases of supersonic flow with near-adiabatic conditions, and of hypersonic flow with severely cooled wall. The DNS results are carried out with an in-house solver [35], which exploits the recycling-rescaling procedure to feed the inflow turbulence. Results obtained with the proposed NSF are compared with those obtained using a standard hyperbolic-sine stretching function (HSF), up to the boundary layer edge. The HSF function is defined as

$$y^+(j) = Re_\tau \frac{\sinh\left(\beta\, j/N_{y,\delta}\right)}{\sinh\beta}, \tag{13}$$

with Re_τ the target friction Reynolds number and β a parameter controlling the intensity of wall clustering. Outside the boundary layer, a geometrical progression is used in both cases, with progression factor of about 1.02. Computational details as flow initialization and procedure for collecting the flow statistics are described by Ceci et al. [24]. In any case, time convergence of the statistical ensembles has been thoroughly checked, and the estimated error for the most sensitive property, namely the peak streamwise velocity variance, is about 0.3%. The relevant parameters for the two flow cases are listed in Table 2.

3.1. Supersonic boundary layer (flow case M2)

The NSF herein designed for the supersonic case is shown in Fig. 1(a), where we assume $\Delta y_w^+ = 0.5$ ($\Delta y_w^* = 0.5$), $j_b = 80$, and with $\alpha_{\rm opt}^* = 2.213$, as found from numerical optimization, given the restriction $\Delta y^+/\eta^+ \leq 2$. The number of points needed to achieve the target friction Reynolds number is in this case $N_{y,\delta} = 178$. In the figure we also report the asymptotic near-wall and outer-layer stretching functions resulting from Eq. (10). For reference, DNS at the same flow conditions has also been carried out using a standard hyperbolic sine stretching function with $\beta = 3.326$, and using $N_{y,\delta} = 293$ grid points, to meet the same resolution requirement as for NSF. The hyperbolic sine mapping is shown in Fig. 1(b). Comparison of the

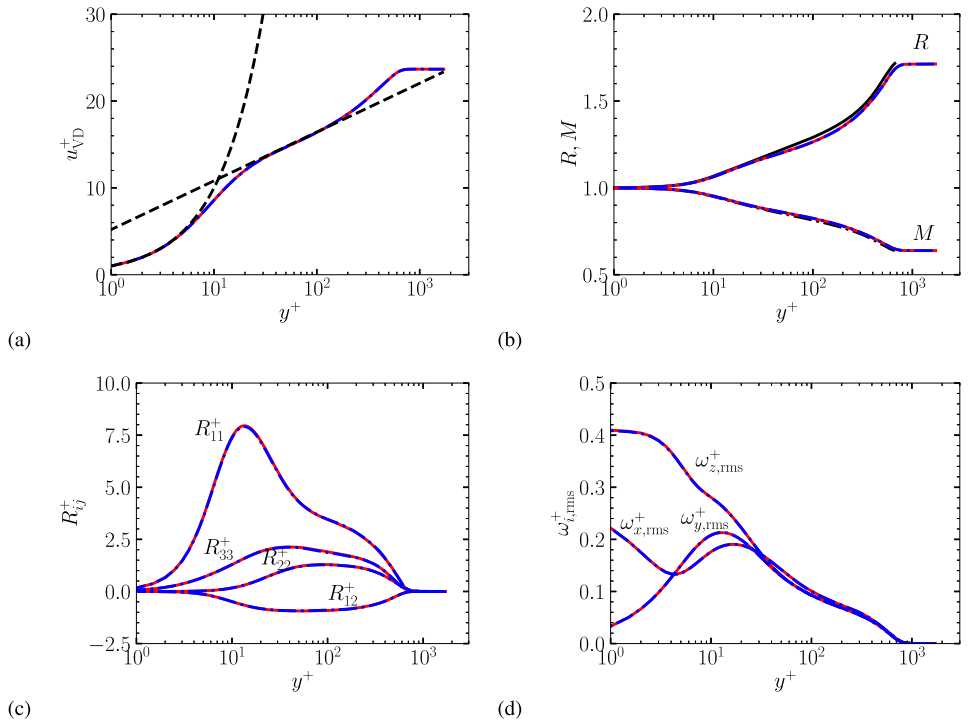

Fig. 3. Flow case M2: van Driest-transformed mean velocity profile (a), mean density and viscosity (b), density-scaled Reynolds stresses (c) and rms of vorticity components (d), using the natural stretching function (red solid lines) and the hyperbolic sine stretching function (blue dash-dotted lines). The dashed black lines in (a) denote the standard laws of the wall $u^+ = y^+$ and $u^+ = 1/\kappa \log(y^+) + C$, with $\kappa = 0.41$ and $C = 5.2$. The black solid line and the black dash-dotted line in (b) show, respectively, the predicted distribution of R and M by Kumar and Larsson [30].

two panels shows earlier deviation of the NSF from the near-wall asymptote, which makes up for a higher number of grid points in the HSF.

As a preliminary assessment of the hypotheses made so far, in Fig. 2(a) we show the local Kolmogorov length scale as a function of the wall-normal distance, as determined from the DNS (solid and dash-dotted lines), and as estimated from Eq. (8) (dotted line). It appears that, despite the assumptions made to arrive at the predictive equation, including approximate distributions of R and M, the correct trend is very well predicted, starting at $y^+ \approx 20$, and all the way through the (near) logarithmic layer. With no surprise, differences arise in the near-wall region and towards the edge of the boundary layer, where the assumption of equilibrium between production and dissipation of turbulence kinetic energy is not satisfied. Verification of this assumption clearly corroborates the whole analysis. In Fig. 2 we show the effective local grid resolution for the NSF and the HSF. One should note here that the resolution requirement for the two stretching is obviously enforced based on the predicted distribution of η. Here the resolution is reported in terms of the actual η determined in the DNS, hence the normalize grid spacing does locally exceed this threshold, however by a very small amount (the maximum is 2.045 for the NSF). The figure well illustrates large differences in the inner part of the wall layer, in which the hyperbolic sine mapping retains unnecessarily small grid spacing also far from the wall, with associated inefficient allocation of grid points.

The basic flow statistics obtained with the two stretching functions are compared in Fig. 3, which includes the van Driest-transformed mean velocity profiles, the mean thermodynamic properties (R and M), the density-scaled Reynolds stresses ($R_{ij} = \overline{\rho}\,\widetilde{u_i'' u_j''}$), and the inner-scaled root-mean-square (rms) vorticity components, the latter being representative of the small-scale flow organization. As shown by Pirozzoli and Bernardini [9], the van Driest transformation here yields good collapse to the incompressible log law, with differences between the two grids of the order of 0.02%. Panel (b) also shows that the model of Kumar and Larsson [30] can predict the mean density and viscosity distributions quite well, with a maximum error of 2.3% and 1.2% on R and M, respectively. As a general comment we can conclude that there is no significant dependence of the statistics herein presented on the type of stretching function, despite the vastly different distribution of the grid points (see again Fig. 1). In fact quantitative scrutiny of the flow statistics shows differences of at most 1% in the Reynolds stresses, whereas differences in the rms vorticities are no more than 0.5%.

3.2. Hypersonic boundary layer (flow case M6)

The NSF function designed for the hypersonic case is shown in Fig. 4(a), where we assume $\Delta y^+_w = 0.50$ ($\Delta y^*_w = 0.47$), $j_b = 80$ and the optimal outer resolution parameter $\alpha^*_{\rm opt} = 3.049$, determined by enforcing the restriction $\Delta y^+/\eta^+ \leq 2$. The

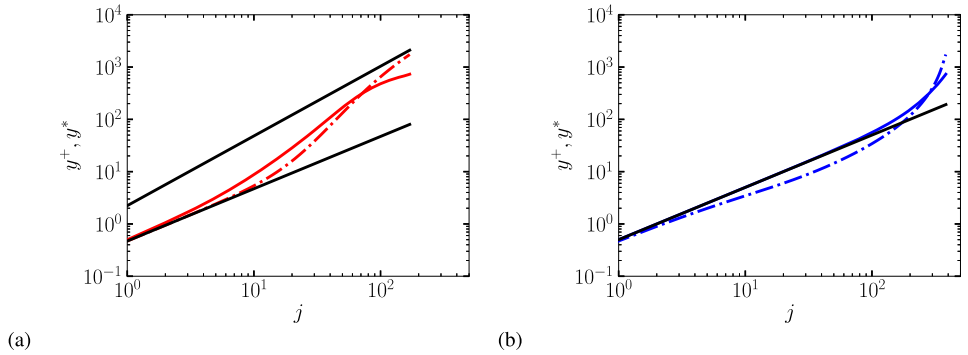

Fig. 4. Flow case M6: natural stretching function (a) and hyperbolic sine stretching function (b). The natural stretching function is designed according to Eqs. (10), (7), assuming $\Delta y_w^+ = 0.50$, $\alpha_{\rm opt}^* = 3.049$. The hyperbolic stretching is designed according to Eq. (13) with $Re_\tau = 730$ and $\beta = 3.194$. The colored solid lines refer to coordinates expressed in wall units (y^+), and the dash-dotted to coordinates expressed in semi-local units (y^*). The black lines in (a) denote the asymptotic near-wall and outer-layer stretching, and in (b) the near-wall stretching only, in wall units.

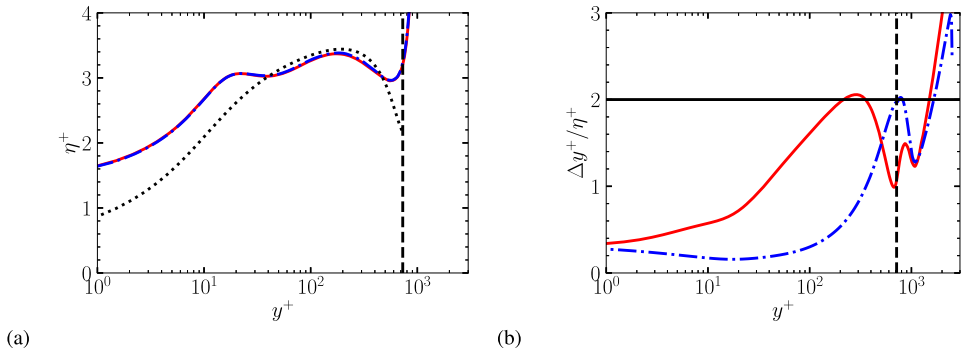

Fig. 5. Flow case M6: distribution of Kolmogorov length scale (a), and grid spacing distribution in local Kolmogorov units (b). In panel (a) the colored lines denote the distribution obtained from the DNS, and the black dotted line the prediction of Eq. (8). In both panels the red solid line indicates the NSF, the blue dash-dotted line the HSF, and the vertical dashed lines mark the boundary layer edge. In panel (b) the black horizontal line denotes the nominal resolution threshold ($\Delta y^+/\eta^+ = 2$).

number of points needed to achieve the target friction Reynolds number is in this case $N_{y,\delta} = 171$. DNS at the same flow conditions has also been carried out using a standard hyperbolic sine stretching function with $\beta = 3.194$, using $N_{y,\delta} = 384$ grid points to meet the same resolution requirement as for NSF. The hyperbolic sine mapping is shown in Fig. 4(b). As in the supersonic case, the figure confirms that the HSF stays close to the linear near-wall stretching over a much wider range, with subsequent inefficient allocation of grid points. The figure also shows larger differences between y^+ and y^*, resulting from variation of the mean thermodynamic properties across the boundary layer. In Fig. 5(a) we show the local Kolmogorov length scale as a function of the wall-normal distance, as computed from the DNS (solid and dash-dotted lines), and as estimated from Eq. (8) (dotted line). Just like in the supersonic flow case we note that, despite expected deviations towards the wall and the edge of the boundary layer, the distribution of η is correctly predicted starting at $y^+ \approx 30$ and up to $y/\delta \approx 0.7$. This is quite remarkable, given the strongly cooled wall condition, and it the basis for success of all following steps. The effective local grid resolution for the NSF and the HSF is shown in Fig. 5(b). Also in this case the actual grid spacing locally exceeds the predetermined threshold, however by a very small amount (the maximum is 2.057 in the NSF). The figure well illustrates large differences in the inner part of the wall layer, in which the hyperbolic sine mapping retains unnecessarily small grid spacing also far from the wall, with even more inefficient allocation of grid points than in the supersonic case.

The basic flow statistics obtained with DNS using the two stretching functions are compared in Fig. 6. First, we note that predictions of the mean flow properties by Kumar and Larsson [30] are still quite accurate, with maximum difference of about 3.3% in the peak viscosity, a bit more than in the supersonic case. The density profiles instead exhibit a maximum difference of 1.8% in the log layer, and depart significantly from the actual distributions towards the boundary layer edge. Again, despite the vastly different distribution of the grid points (see Fig. 4), the two DNS yield a prediction of the mean and fluctuating statistics to within less than 1% (the error is maximum for the Reynolds stresses), which is of the same order as the uncertainty in the statistical averaging.

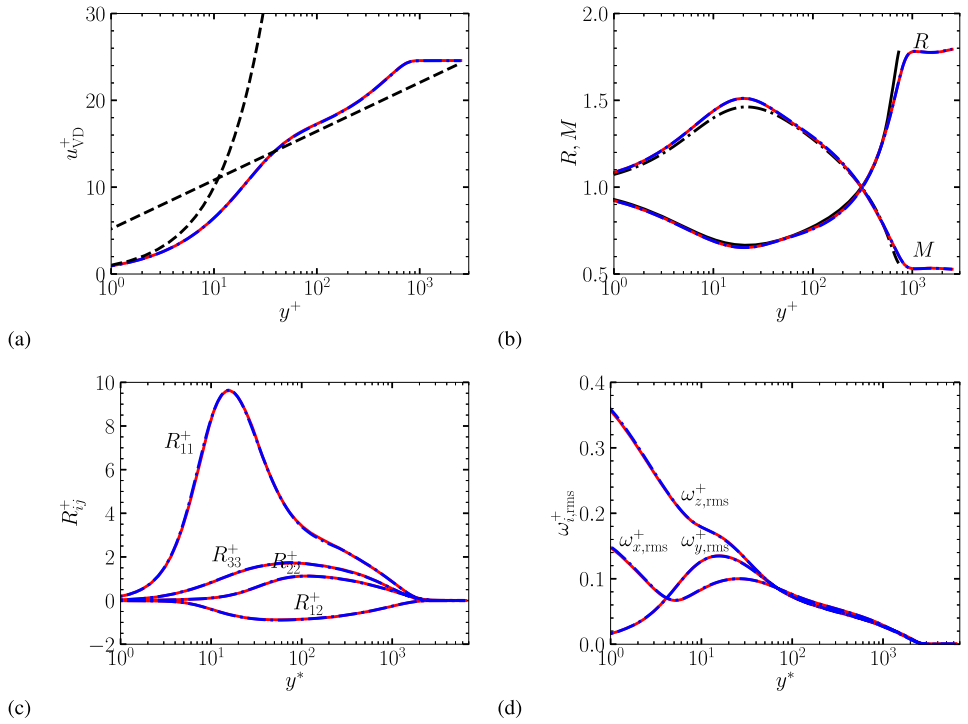

Fig. 6. Flow case M6: van Driest-transformed mean velocity profile (a), mean density and viscosity (b), density-scaled Reynolds stresses (c) and rms of vorticity components (d), using the natural stretching function (red solid lines) and the hyperbolic sine stretching function (blue dash-dotted lines). The dashed black lines in (a) denote the standard laws of the wall $u^+ = y^+$ and $u^+ = 1/\kappa \log(y^+) + C$, with $\kappa = 0.41$ and $C = 5.2$. The black solid line and the black dash-dotted line in (b) show, respectively, the predicted distribution of R and M by Kumar and Larsson [30].

Table 3
List of computational parameters for the wall-normal grid refinement study. NSF refers to the proposed natural stretching function, and HSF refers to hyperbolic sine stretching function. Here N_x, N_y, N_z are the number of collocation points in the streamwise, wall-normal and spanwise directions. $N_{y,\delta}$ is the number of grid points in the wall-normal direction up to the boundary layer edge. The NSF simulations are characterized by the grid transition parameter j_b, the optimal value of the resolution parameter (α^*_{opt}) and its maximum value (α_{max}). The HSF grids are characterized in terms of the stretching parameter (β) and α_{max}.

Flow case	M_0	Re_τ	$N_x \times N_y \times N_z$	$N_{y,\delta}$	j_b	α_{max}	α^*_{opt}	β
M2-NSF	2.00	610	$4016 \times 272 \times 560$	178	80	2.045	2.213	–
M2-NSF-A1	2.00	610	$4016 \times 212 \times 560$	147	80	2.564	2.854	–
M2-NSF-A2	2.00	610	$4016 \times 160 \times 560$	104	80	3.310	3.904	–
M2-HSF	2.00	610	$4016 \times 368 \times 560$	293	–	2.110	–	3.326
M2-HSF-B1	2.00	610	$4016 \times 212 \times 560$	147	–	5.297	–	4.263
M2-HSF-B2	2.00	610	$4016 \times 160 \times 560$	104	–	7.651	–	4.479
M6-NSF	5.84	730	$5024 \times 288 \times 560$	171	80	2.057	3.049	–
M6-NSF-A1	5.84	730	$5024 \times 220 \times 560$	135	80	2.586	4.145	–
M6-NSF-A2	5.84	730	$5024 \times 180 \times 560$	103	80	3.360	6.118	–
M6-HSF	5.84	730	$5024 \times 496 \times 560$	384	–	2.024	–	3.194
M6-HSF-B1	5.84	730	$5024 \times 220 \times 560$	135	–	7.431	–	4.601
M6-HSF-B2	5.84	730	$5024 \times 180 \times 560$	103	–	10.01	–	4.947

4. Wall-normal grid refinement study

The effect of wall-normal resolution is herein considered by changing the threshold of the α parameter. Four additional supersonic and four hypersonic DNS have been carried out, according to the following reasoning: first, we selected different threshold values of α to generate two coarser NSF wall-normal meshes, with associated $N_{y,\delta}$ and N_y; the same grid points are then used to generate the HSF meshes. This way we can separately establish the effect of resolution on NSF wall-normal points distribution, and compare grid generation strategies. Obviously, by setting the same resolution constraint, a higher number of grid points is needed for HSF, whereas setting the same number of points yields higher values of α. The flow parameters for the additional DNS are listed in Table 3. The size of the computational box, flow initialization, inflow turbulence forcing and flow statistics collection are the same as in the baseline DNS.

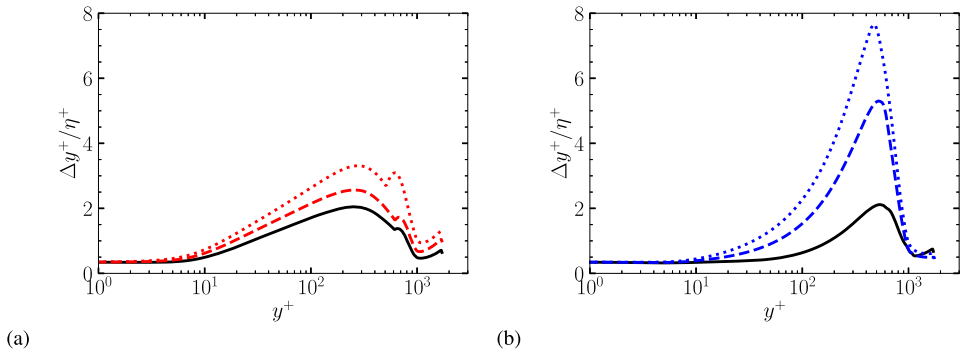

Fig. 7. Flow case M2: grid spacing distribution in local Kolmogorov units for NSF meshes (a) and HSF meshes (b). The colored dashed lines refer to the distributions with $N_y = 212$ (M2-NSF-A1 and M2-HSF-B1), and the colored dotted lines to $N_y = 160$ (M2-NSF-A2 and M2-HSF-B2). The solid black lines denote the baseline meshes (M2-NSF and M2-HSF).

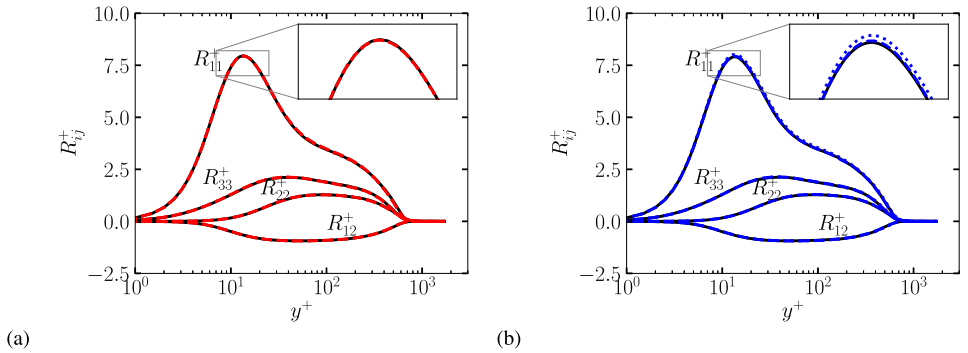

Fig. 8. Flow case M2: density-scaled Reynolds stresses for the NSF meshes (a) and HSF meshes (b). The colored dashed lines refer to the distributions with $N_y = 212$ (M2-NSF-A1 and M2-HSF-B1), and the colored dotted lines to $N_y = 160$ (M2-NSF-A2 and M2-HSF-B2). The solid black lines denote the baseline meshes (M2-NSF and M2-HSF).

4.1. Grid refinement

The effect of grid refinement is considered first, starting from the supersonic flow case. Two grids have been generated, by setting the threshold of α to 2.5 and 3.25, which yields respectively $\alpha^*_{\text{opt}} = 2.854, 3.904$, $N_{y,\delta} = 147, 104$, $N_y = 212, 160$, which are then considered to generate the HSF grids. Enforcement of $N_{y,\delta}$, N_y however gives no control of the β parameter, which therefore has to be adjusted to $\beta = 4.263, 4.479$. In Fig. 7 we show the grid spacing distribution for the baseline and coarsened NSF meshes (panel a) and HSF meshes (panel b). Spacings as high as $\Delta y^+/\eta^+ \approx 5 - 8$ result for the HSF meshes.

The resulting density-scaled Reynolds stress profiles are shown in Fig. 8. The most sensitive resolution indicator is the peak of the streamwise stress, for which differences with respect to the baseline case are of about 0.15% for the NSF meshes, which is within the statistical sampling error. On the other hand, the peak is overestimated by 0.35% for the M2-HSF-B1 mesh and by 1.6% for the M2-HSF-B2 mesh.

The same analysis was repeated for the hypersonic flow conditions. Two new meshes were again generated by setting the threshold of α to 2.5 and 3.25, which respectively yields $\alpha^*_{\text{opt}} = 4.145, 6.118$, $N_{y,\delta} = 135, 103$ and $N_y = 220, 180$. The latter values of $N_{y,\delta}$ and N_y have been used to generate equivalent HSF distributions, with hyperbolic stretching parameters $\beta = 4.601, 4.947$. In Fig. 9 we show the grid spacing distribution in local Kolmogorov units for the baseline and for the coarsened NSF meshes (panel a) and HSF meshes (panel b). In this case, the HSF mesh has wall-normal spacing up to $\Delta y^+/\eta^+ \approx 7.5 - 10$ within the boundary layer.

The resulting density-scaled Reynolds stress profiles are shown in Fig. 10. Differences of the peak longitudinal stress with respect to the baseline case are 0.21% for the M6-NSF-A1 mesh, and 0.55% for the M6-NSF-A2 mesh. The peak is overestimated by 0.25% for the M6-HSF-B1 mesh and by 1.2% for the M6-HSF-B2 mesh.

5. Conclusions

We have formulated an extension of the natural grid stretching approach introduced by Pirozzoli and Orlandi [5] for incompressible flow, to compressible boundary layers, which allows to automatically generate wall-normal grid mapping functions and associated number of grid points, for arbitrarily prescribed flow conditions, in terms of Reynolds and Mach number, and wall cooling ratio. Just like in the incompressible case, we argue that a physics-driven stretching functions for

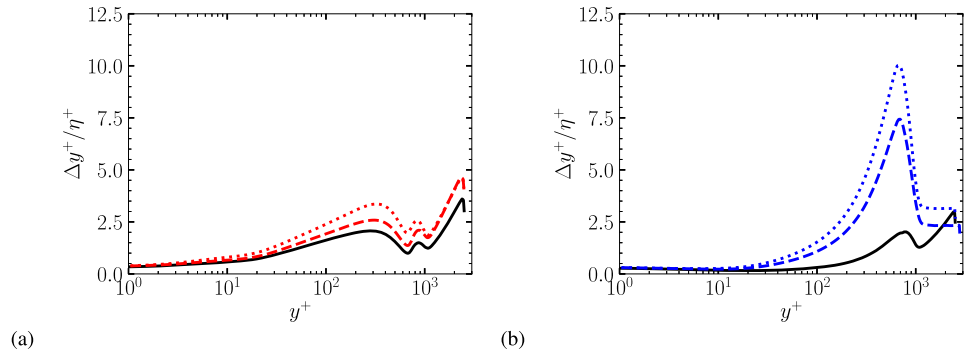

Fig. 9. Flow case M6: grid spacing distribution in local Kolmogorov units for NSF meshes (a) and HSF meshes (b). The colored dashed lines refer to the distributions with $N_y = 220$ (M6-NSF-A1 and M6-HSF-B1), and the colored dotted lines to $N_y = 180$ (M6-NSF-A2 and M6-HSF-B2). The solid black lines denote the baseline meshes (M6-NSF and M6-HSF).

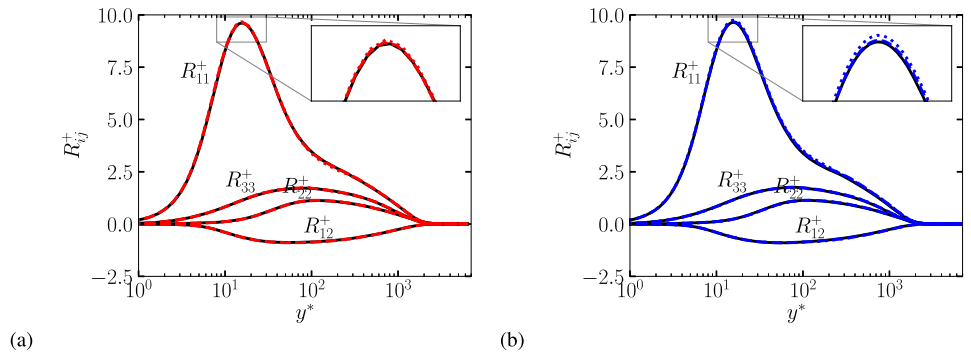

Fig. 10. Flow case M6: density-scaled Reynolds stresses for the NSF meshes (a) and HSF meshes (b). The colored dashed lines refer to the distribution with $N_y = 220$ (M6-NSF-A1 and M6-HSF-B1), and the colored dotted lines to $N_y = 180$ (M6-NSF-A2 and M6-HSF-B2). The solid black lines denote the baseline meshes (M6-NSF and M6-HSF).

wall-bounded flows should patch an inner-layer stretching with an outer-layer stretching, in which the grid spacing should be proportional to the local Kolmogorov length scale. The basic assumptions which allow extension to the compressible case are universality of the mapping in terms of semi-local coordinates, and local equilibrium in the outer layer, which allows to predict the dissipative length scale according to Eq. (8). An important building block is also the availability of reliable profiles of the mean flow properties, for which we rely on the work of Kumar and Larsson [30]. The formulated setup is not restricted to any particular flow or wall condition but can range from supersonic to hypersonic flows, also in the presence of substantial wall heat flux. By construction, the mapping has the natural property of yielding precisely constant resolution in terms of the semi-local Kolmogorov length scale. For that purpose, the resolution parameter α^*_{opt} is designed in such a way that the resolution does not exceed the desired threshold in local Kolmogorov units in the outer part of the wall layer, where turbulence is nearly isotropic. The outer-layer stretching is combined with a near-wall uniformly-spaced distribution by means of a blending function controlled by the parameter j_b, which sets the number of grid points within the buffer layer. Although DNS are shown here only for the case of boundary layers, the same mapping can also be adapted with minimal modifications to study channel and pipe flows.

A grid refinement study in the wall-normal direction was conducted in order to assess the sensitivity of the proposed NSF to the choice of the threshold for the resolution parameter (α), and to compare NSF and HSF meshes with the same number of points. Despite significant differences in the wall-normal stretching, all distributions yield results close to the baseline case, with exception of the coarsest HSF meshes. This result is very interesting, but it raises questions regarding the influence of the resolution peak value and its position within the boundary layer on the computed flow statistics. In fact, HSF meshes still yield satisfactory results although high values of α are attained towards the edge of the boundary layer.

We believe that our grid stretching strategy can be useful in future DNS of compressible flows at high Reynolds number as in our tests, it allows fewer grid points along the wall-normal direction for given resolution compared to other stretching functions, with subsequent judicious exploitation of the computational resources. We also believe that the procedure presented in this paper can be profitably applied to numerical simulations based on the LES paradigm, both in the wall-resolved and in the wall-modeled mode [36]. In the first case, the very same composite natural transformation described here can be used, by suitably increasing the threshold value of the resolution parameter. In the second case, one could rely on the outer wall stretching alone, since the near-wall region is modeled.

Some limitations of this study should be at the same time clearly stated. In fact, whereas available evidence shows that the same resolution requirements apply to incompressible flow and to the solenoidal part of the velocity field in compressible flow in the presence of strong compressibility effects, dilatational modes become dynamically important, and should be adequately resolved [22]. These effects are disregarded in the present work, but could be an interesting subject for future research.

A modular Python implementation of the proposed stretching is available on the github repository HYPERGRID [37]. The original modules used to compute the boundary layer profiles can be found at the web page https://larsson.umd.edu/code/ (compressibleBLprofiles).

CRediT authorship contribution statement

Alessandro Ceci: Investigation, Software, Writing – original draft. **Sergio Pirozzoli:** Conceptualization, Writing – review & editing.

Declaration of competing interest

The authors declare that they have no known competing financial interests or personal relationships that could have appeared to influence the work reported in this paper.

Data availability

Data will be made available on request.

Acknowledgements

This work was supported by TEAMAero Horizon 2020 research and innovation program under grant agreement 860909 and by the Air Force Office of Scientific Research under grant FA9550-19-1-7029. We acknowledge that the results reported in this paper have been achieved with computational resources of the PRACE Research Infrastructure resource MARCONI100 based at CINECA, Casalecchio di Reno, Italy. We would like to thank Johan Larsson and Vedant Kumar of the University of Maryland for kindly agreeing to share their Python script for the generation of the mean flow profiles.

References

[1] J. Kim, P. Moin, R. Moser, Turbulence statistics in fully developed channel flow at low Reynolds number, J. Fluid Mech. 177 (1987) 133–166.
[2] M. Lee, R. Moser, Direct simulation of turbulent channel flow layer up to $\mathrm{Re}_\tau = 5200$, J. Fluid Mech. 774 (2015) 395–415.
[3] P. Orlandi, The importance of wall-normal Reynolds stress in turbulent rough channel flows, Phys. Fluids 25 (2013) 110813.
[4] M. Bernardini, S. Pirozzoli, P. Orlandi, Velocity statistics in turbulent channel flow up to $\mathrm{Re}_\tau = 4000$, J. Fluid Mech. 742 (2014) 171–191.
[5] S. Pirozzoli, P. Orlandi, Natural grid stretching for DNS of wall-bounded flows, J. Comput. Phys. 439 (2021) 110408.
[6] L. Duan, I. Beekman, M.P. Martin, Direct numerical simulation of hypersonic turbulent boundary layers. Part 2. Effect of wall temperature, J. Fluid Mech. 655 (2010) 419–445.
[7] L. Duan, I. Beekman, M.P. Martin, Direct numerical simulation of hypersonic turbulent boundary layers. Part 3. Effect of Mach number, J. Fluid Mech. 672 (2011) 245–267.
[8] M. Lagha, J. Kim, J. Eldredge, X. Zhong, A numerical study of compressible turbulent boundary layers, Phys. Fluids 23 (2011) 015106.
[9] S. Pirozzoli, M. Bernardini, Turbulence in supersonic boundary layers at moderate Reynolds number, J. Fluid Mech. 688 (2011) 120–168.
[10] C. Wenzel, B. Selent, M. Kloker, U. Rist, DNS of compressible turbulent boundary layers and assessment of data/scaling-law quality, J. Fluid Mech. 842 (2018) 428–468.
[11] C. Zhang, L. Duan, M.M. Choudhari, Direct numerical simulation database for supersonic and hypersonic turbulent boundary layers, AIAA J. 56 (2018) 4297–4311.
[12] J. Huang, L. Duan, M.M. Choudhari, Direct numerical simulation of hypersonic turbulent boundary layers: effect of spatial evolution and Reynolds number, J. Fluid Mech. 937 (2022) A3.
[13] M. Cogo, F. Salvadore, F. Picano, M. Bernardini, Direct numerical simulation of supersonic and hypersonic turbulent boundary layers at moderate-high Reynolds numbers and isothermal wall condition, J. Fluid Mech. 945 (2022).
[14] J. Jiménez, Coherent structures in wall-bounded turbulence, J. Fluid Mech. 842 (2018) P1.
[15] S. Hoyas, J. Jiménez, Scaling of velocity fluctuations in turbulent channels up to $Re_\tau = 2003$, Phys. Fluids 18 (2006) 011702.
[16] J. Jiménez, A.A. Wray, On the characteristics of vortex filaments in isotropic turbulence, J. Fluid Mech. 373 (1998) 255–285.
[17] A. Lozano-Durán, J. Jiménez, Effect of the computational domain on direct simulations of turbulent channels up to $\mathrm{Re}_\tau = 4000$, Phys. Fluids 26 (2014) 011702.
[18] X. Wu, P. Moin, A direct numerical simulation study on the mean velocity characteristics in turbulent pipe flow, J. Fluid Mech. 608 (2008) 81–112.
[19] C. Chin, J. Monty, A. Ooi, Reynolds number effects in DNS of pipe flow and comparison with channels and boundary layers, Int. J. Heat Fluid Flow 45 (2014) 33–40.
[20] J. Ahn, J. Lee, H. Jae, J. Lee, J.-H. Kang, H. Sung, Direct numerical simulation of a 30R long turbulent pipe flow at $\mathrm{Re}_\tau = 3008$, Phys. Fluids 27 (2015) 065110.
[21] S. Pope, Turbulent Flows, Cambridge University Press, 2000.
[22] M. Yu, C.-X. Xu, S. Pirozzoli, Genuine compressibility effects in wall-bounded turbulence, Phys. Rev. Fluids 4 (2019) 123402.
[23] S. Pirozzoli, M. Bernardini, Probing high-Reynolds-number effects in numerical boundary layers, Phys. Fluids 25 (2013) 021704.
[24] A. Ceci, A. Palumbo, J. Larsson, S. Pirozzoli, Numerical tripping of high-speed turbulent boundary layers, Theor. Comput. Fluid Dyn. 36 (2022).
[25] P. Orlandi, Fluid Flow Phenomena: A Numerical Toolkit, Kluwer, 2000.

[26] P. Huang, G. Coleman, P. Bradshaw, Compressible turbulent channel flows: DNS results and modeling, J. Fluid Mech. 305 (1995) 185–218.
[27] A. Patel, J.W. Peeters, B.J. Boersma, R. Pecnik, Semi-local scaling and turbulence modulation in variable property turbulent channel flows, Phys. Fluids 27 (2015).
[28] A. Trettel, J. Larsson, Mean velocity scaling for compressible wall turbulence with heat transfer, Phys. Fluids 28 (2016).
[29] R. Pecnik, A. Patel, Scaling and modelling of turbulence in variable property channel flows, J. Fluid Mech. 823 (2017).
[30] V. Kumar, J. Larsson, Modular method for estimation of velocity and temperature profiles in high-speed boundary layers, AIAA J. (2022) 1–8.
[31] E.R. Van Driest, On turbulent flow near a wall, J. Aeronaut. Sci. 23 (1956).
[32] D. Coles, The law of the wake in the turbulent boundary layer, J. Fluid Mech. 1 (1956) 191–226.
[33] P.S. Volpiani, P.S. Iyer, S. Pirozzoli, J. Larsson, Data-driven compressibility transformation for turbulent wall layers, Phys. Fluids 5 (2020) 052602.
[34] D. Modesti, S. Pirozzoli, An efficient semi-implicit solver for direct numerical simulation of compressible flows at all speeds, J. Sci. Comput. 75 (2018) 308–331.
[35] M. Bernardini, D. Modesti, F. Salvadore, S. Pirozzoli, Streams: a high-fidelity accelerated solver for direct numerical simulation of compressible turbulent flows, Comput. Phys. Commun. 263 (2021) 107906.
[36] J. Larsson, S. Kawai, J. Bodart, I. Bermejo-Moreno, Large eddy simulation with modeled wall-stress: recent progress and future directions, Mech. Eng. Rev. 3 (2016) 15–00418.
[37] A. Ceci, V. Kumar, J. Larsson, S. Pirozzoli, HYPERGRID, https://github.com/a-ceci/HYPERGRID, 2022.